ChemPubSoc Europe

DOI: 10.1002/chem.201502952

CHEMISTRY A European Journal Full Paper

Electrochemistry

Controlled Redox Chemistry at Cerium within a Tripodal Nitroxide Ligand Framework

Justin A. Bogart,[a] Connor A. Lippincott,[a] Patrick J. Carroll,[a] Corwin H. Booth,[b] and Eric J. Schelter*[a]

Abstract: Ligand reorganization has been shown to have a profound effect on the outcome of cerium redox chemistry. Through the use of a tethered, tripodal, trianionic nitroxide ligand, $[((2\text{-}t\text{BuNO})C_6H_4CH_2)_3N]^{3-}$ ($TriNO_x^{3-}$), controlled redox chemistry at cerium was accomplished, and typically reactive complexes of tetravalent cerium were isolated. These included rare cationic complexes $[Ce(TriNO_x)thf][BAr^F{}_4]$, in which $Ar^F = 3,5\text{-}(CF_3)_2\text{-}C_6H_3$, and $[Ce(TriNO_x)py][OTf]$. A rare complete Ce–halide series, $Ce(TriNO_x)X$, in which $X = F^-$, Cl^-, Br^-, I^-, was also synthesized. The solution chemistry of these complexes was explored through detailed solution-phase electrochemistry and ^1H NMR experiments and showed a unique shift in the ratio of species with inner- and outer-sphere anions with size of the anionic X^- group. DFT calculations on the series of calculations corroborated the experimental findings.

Introduction

A recent survey of the literature by our group showed that the redox properties of cerium(III) are highly sensitive to ligand field.[1] For example, exchanging the weakly coordinating nitrate ligands in ceric ammonium nitrate ($E_{1/2} = 1.21$ V vs. Fc/Fc^+) with catecholate ligands in $[Ce(O_2C_6H_4)_4]^{4-}$ ($E_{1/2} = -0.85$ V vs. Fc/Fc^+) changed the cerium cation from a potent oxidant to a potent reductant.[2] Understanding of the ability to tune the redox potential of cerium has broad applications in energy science,[3] separations chemistry,[4] and organic synthesis.[2b] This has motivated renewed interest by us and others in studying the coordination chemistry of cerium in the 4+ oxidation state.[5]

Few studies have explored the coordination chemistry of Ce^{IV} in tripodal, trianionic ligand environments.[6] In a seminal study by Scott and co-workers, use of the silyl substituted tris(2-aminoethyl)amine ligand, $[N(CH_2CH_2N(SiMe_2t\text{Bu}))_3]^{3-}$ (NN'_3), afforded isolation of the Ce^{IV} oxidation state, in particular of the $CeI(NN'_3)$ complex. However, in the cases of Cl^- and Br^-, the stability of the 4+ oxidation state was not sufficient to prevent formation of the mixed valent $Ce^{III/IV}$ dimers, $[Ce(NN'_3)]_2(\mu\text{-}X)$, $X = Cl^-$, Br^-.[6a] In contrast, extensive studies have been performed on the coordination chemistry of tripodal trianionic ligands to various transition metals, as well as uranium in the f block (Figure 1).[7]

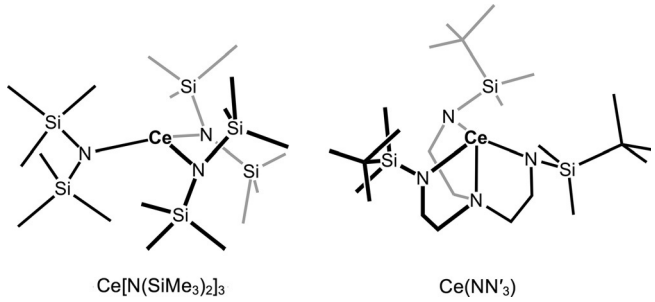

Figure 1. Published tris-silylamide complexes of cerium.

The coordination and redox chemistry of cerium within the related, untethered $Ce[N(SiMe_3)_2]_3$ system have also been studied. Unlike the $Ce(NN'_3)$ system, no reaction occurred upon addition of molecular halogens to $Ce^{III}[N(SiMe_3)_2]_3$ ($Ce^{III/IV}$ $E_{1/2} = 0.35$ V vs. Fc/Fc^+).[6a,8] Although $CeI(NN'_3)$ could be formed through oxidation with molecular I_2, an analogous reaction in the formation of $CeI[N(SiMe_3)_2]_3$ did not occur. In fact, $CeI[N(SiMe_3)_2]_3$ was formed through a halide-transfer reaction from a cerium(IV) precursor, $CeF[N(SiMe_3)_2]_3$, using $Me_3Si\text{–}I$ rather than through oxidation of $Ce^{III}[N(SiMe_3)_2]_3$.[5f] Scott and co-workers postulated that the increased stability of the Ce^{IV} state in their tethered $Ce(NN'_3)$ systems compared to $Ce[N(SiMe_3)_2]_3$ system was a result of reduced ligand reorganization involved in accommodating the X^- ligand in the former. Indeed, ligand reorganization has been shown to have profound effects on the redox chemistry at cerium.[5c] As was shown by Anwander and co-workers, oxidation of $Ce[N(SiHMe_2)_2]_3(thf)_2$ with chlorinating agents in THF led to the clean formation of $Ce[N(SiHMe_2)_2]_4$ through ligand redistribution pathways. However,

[a] J. A. Bogart, C. A. Lippincott, Dr. P. J. Carroll, Prof. E. J. Schelter
P. Roy and Diana T. Vagelos Laboratories
Department of Chemistry, University of Pennsylvania
231 S. 34th St., Philadelphia, PA 19104 (USA)
E-mail: schelter@sas.upenn.edu

[b] Dr. C. H. Booth
Chemical Sciences Division
Lawrence Berkeley National Laboratory
Berkeley, CA 94720 (USA)

Supporting information for this article is available on the WWW under http://dx.doi.org/10.1002/chem.201502952.

performing the same reaction in donor-free solvents led to the formation of the $Ce_5[N(SiHMe_2)_2]_8Cl_7$ cluster and other intractable products.[5k] In this context, there is a clear need to expand the coordination chemistry of cerium using strongly donating, tethered tripodal systems, in which the reduced ligand reorganization effects would confer stability to the Ce^{IV} oxidation state.

Recently, we communicated the synthesis of the tripodal trianionic nitroxide, $[((2\text{-}t\text{BuNOH})C_6H_4CH_2)_3N]^{3-}$ ($TriNO_x^{3-}$), and its coordination chemistry with the rare-earth elements La, Nd, Dy, and Y.[9] The η^2-(N,O) binding mode of the three ligand arms provided a single coordination site for substrate binding. Previous studies by our group showed that nitroxide ligand fields provided significant stabilization to the Ce^{IV} state through increased electron donation into the empty metal 4f orbitals from the well energy matched N–O π^* orbitals.[5b,10] We hypothesized that the environment of $TriNO_x^{3-}$ would impart an improved stabilization to the Ce^{IV} state compared to the tren framework while providing a single coordination site to elucidate controlled redox chemistry.

Herein, we report the synthesis of the monomeric $Ce^{III}(TriNO_x)$thf (**1**) and dimeric $[Ce^{III}(TriNO_x)]_2$ (**2**), analogues of the previously published M($TriNO_x$)thf, M = La, Nd, Dy, and Y, and $[M(TriNO_x)]_2$, M = La and Nd, complexes. Ce^{IV} complexes, [Ce(TriNOx)thf][$BAr^F{}_4$] (**3-BAr$^F_4$**) and [Ce(TriNOx)pyr][OTf] (**3-OTf**), rare examples of crystallographically characterized cationic Ce^{IV} complexes, were accessed from **1**. The complete halide series, Ce($TriNO_x$)X, in which X = F^- (**3-F**), Cl^- (**3-Cl**), Br^- (**3-Br**), and I^- (**3-I**), are also reported.

Detailed characterization of the cerium complexes to understand their coordination chemistries in solution are disclosed. These include solution-phase electrochemistry and ^{1}H NMR spectroscopy experiments. DFT calculations corroborated the experimental findings and provided evidence for 4f orbital mixing in the Ce^{IV} complexes.

Results and Discussion

Synthesis and characterization

The shortage of tridentate frameworks in the literature that stabilize the Ce^{IV} oxidation state prompted us to study the redox chemistry of cerium using the $TriNO_x^{3-}$ framework. The synthesis of the $Ce^{III}(TriNO_x)$thf complex (**1**) was achieved through an analogous route to the previously reported $M^{III}(TriNO_x)$thf complexes, M = La, Nd, Dy, and Y, in which a hexanes solution of $Ce[N(SiMe_3)_2]_3$ was layered onto a THF solution of H_3TriNO_x (Scheme 1, top).[9] X-ray crystallography confirmed **1** was isostructural with the M($TriNO_x$)thf complexes, with retention of the η^2-(N,O) bonding mode of the three nitroxide arms and the coordination of a THF molecule to the central cerium cation (Figure 2, top).

The coordination chemistry of **1** in solution was analogous to the early M cations, M = La and Nd, as indicated by ^{1}H NMR spectroscopy (see the Supporting Information). The [Ce($TriNO_x$)]$_2$ complex (**2**) could be synthesized by dissolving **1** in toluene solution and removing the volatiles under reduced pressure (Scheme 1, bottom). Crystals of **2** suitable for X-ray diffraction analysis were formed by cooling a saturated Et_2O solution of **1** to −25 °C, which confirmed its dimeric structure (Figure 2, bottom).

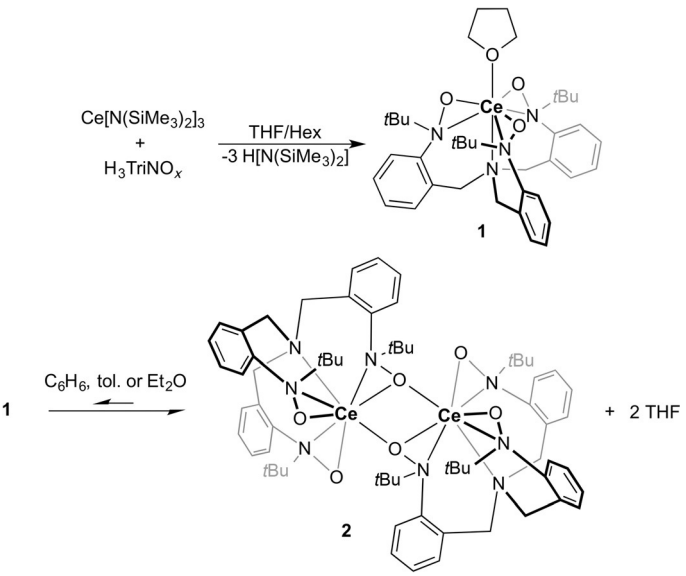

Scheme 1. Schematic of the synthesis of Ce($TriNO_x$)thf (**1**), top, and the self-association equilibrium of **1** to form [Ce($TriNO_x$)]$_2$ (**2**), bottom.

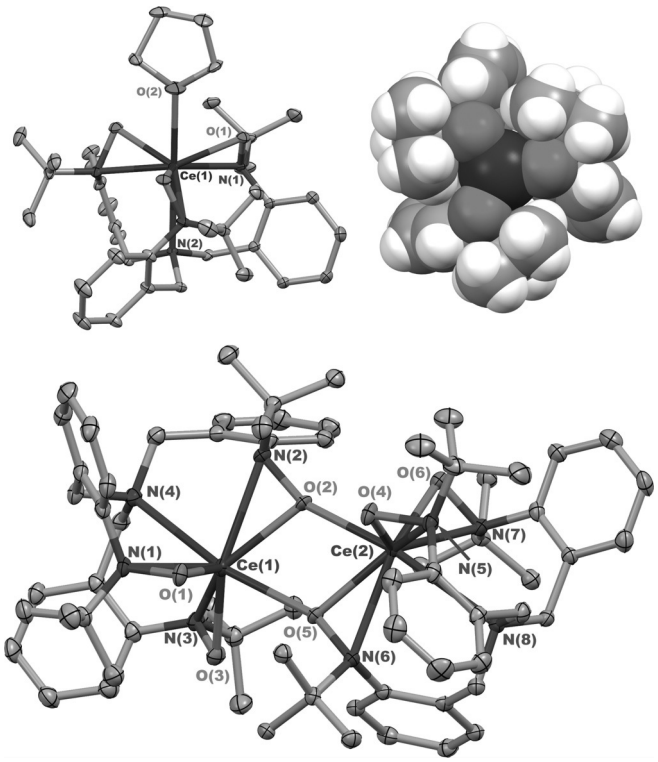

Figure 2. Thermal ellipsoid plot and space-fill diagram of **1** (top) and thermal ellipsoid plot of **2** (bottom). Hydrogen atoms omitted for clarity. Selected bond lengths [Å] for **1**: Ce(1)–O(1) 2.2921(18), Ce(1)–N(1) 2.581(2), Ce(1)–O(2) 2.577(6); for **2**: Ce(1)–O(1) 2.297(3); Ce(1)–O(3) 2.273(3); Ce(1)–O(2) 2.364(3); Ce(1)–N(1) 2.639(3); Ce(1)–N(3) 2.606(3); Ce(1)–N(2) 2.689(3); Ce(1)–O(5) 2.523(3).

To gain insight into the chemically accessible redox states of **1**, electrochemistry experiments were performed in dichloromethane solution. As shown in Figure S19 in the Supporting Information, the cyclic voltammogram of **1** showed only one wave centered at −0.96 V versus Fc/Fc^+ ($E_{pa}=-0.88$ V, $E_{pc}=-1.04$ V). Based on the open circuit potential of −1.14 V, this wave was assigned as the metal-based $Ce^{III/IV}$ redox couple, which was later confirmed chemically through the isolation of a series of Ce^{IV} complexes (see below). The measured potential was compared to that of the $Ce^{III/IV}$ redox couple for $Ce[N(SiMe_3)_2]_3$, which showed a quasi-reversible $Ce^{III/IV}$ wave at $E_{1/2}=0.35$ V versus Fc/Fc^+.[8] This 1.31 V shift in $Ce^{III/IV}$ redox potential between **1** and $Ce[N(SiMe_3)_2]_3$ indicated the stability to the 4+ oxidation state imposed by the $TriNO_x^{3-}$ framework relative to the $[N(SiMe_3)_2]^-$ framework. Furthermore, the peak separation, ΔE, of 0.16 V in **1** compared to approximately 0.5 V in $Ce[N(SiMe_3)_2]_3$ was suggestive of a relatively small ligand reorganization involved in the oxidation of **1** compared to that in the oxidation of $Ce[N(SiMe_3)_2]_3$ (Table 1).

Table 1. Redox potentials of the $Ce^{III/IV}$ couple (in V vs. Fc/Fc^+) for cerium in salient ligand frameworks.

	$E_{1/2}$ $Ce^{III/IV}$	$\Delta E_{1/2}$ $Ce^{III/IV}$	I_{pa}/i_{pc}	Ref.
$[nBu_4N]_2[Ce(NO_3)_6]$	0.62	0.075	–	[11]
$Ce[N(SiMe_3)_2]_3$	0.35	≈0.5	≈2	[12]
CeLiB[a]	−0.76	0.64	1.94	[5c]
$Ce[2\text{-}(t\text{BuNO})py]_4$	−1.80	0.19	0.90	[10]
$Ce(TriNO_x)THF$	−0.96	0.16	1.08	this work

[a] CeLiB = $[M_3(THF)_4][(binolate)_3Ce(THF)]$.

The absence of a second oxidation feature to 1.0 V suggested that the formation of a $[Ce^{IV}(TriNO_x^{2-})]^{2+}$ complex, in which both the metal center and one of the nitroxide arms of the ligand were oxidized, was chemically unfeasible. This result was surprising given the ease at which free H_3TriNO_x was oxidized ($E_{1/2}=-0.55$ V vs. Fc/Fc^+, Figure S18 in the Supporting Information) and indicated that coordination to the highly Lewis acidic Ce^{IV} center stabilized the potential of the $TriNO_x^{3-}$ redox couple by over 1.0 V.

Based on the measured redox potential of cerium within the $TriNO_x^{3-}$ ligand framework, ferrocenium salts were selected as oxidants for controlled oxidation chemistry at the cerium cation. The quasi-reversibility of the $Ce^{III/IV}$ redox wave in the CV of **1** suggested that a cationic $[Ce(TriNO_x)thf]^+$ complex could be isolated. In fact, reaction of **1** with $Fc[BAr^F{}_4]$ in toluene led to the immediate formation of a sparingly soluble dark red brown solid. Crystallization of this complex through vapor diffusion of pentane into a saturated THF solution induced formation of crystals of $[Ce(TriNO_x)thf][BAr^F{}_4]$ (**3-BAr$^F{}_4$**), $Ar^F=3,5\text{-}(CF_3)_2\text{-}C_6H_3$, that were suitable for X-ray diffraction analysis. Similarly, reaction of **1** with Fc[OTf] in toluene led to the formation of an insoluble dark red brown solid. Crystallization of this complex by vapor diffusion of Et_2O into a saturated pyridine solution gave crystals of [Ce(TriNOx)pyr][OTf] (**3-OTf**) suitable for X-ray diffraction analysis (Scheme 2).

Complexes **3-BAr$^F{}_4$** and **3-OTf** are rare examples of structurally characterized cationic cerium complexes. To date, only one other crystallographically characterized cationic Ce^{IV} complex, [(TRENDSAL)Ce][BPh_4], where $TRENDSAL^{3-}$ = $\{N[CH_2CH_2N=CH(C_6H_2t\text{Bu}_2\text{-}3,5\text{-}O\text{-}2]_3\}^{3-}$, has been reported.[13] Similar to $TriNO_x^{3-}$, the Schiff base framework in [(TRENDSAL)Ce][BPh_4] was sufficiently bulky and electron rich to mitigate the strong Lewis acidity of the Ce^{IV} cation and prevent unwanted reactivity. The structural metrics of **3-BAr$^F{}_4$** and **3-OTf** were consistent with the central cerium cation being in the 4+ oxidation state. The N–O bond lengths ranged from 1.418(8) to 1.436(7) Å in **3-BAr$^F{}_4$** and 1.431(4) to 1.435(4) Å in **3-OTf**, which fell in the range of typical anionic nitroxide bond lengths and are similar

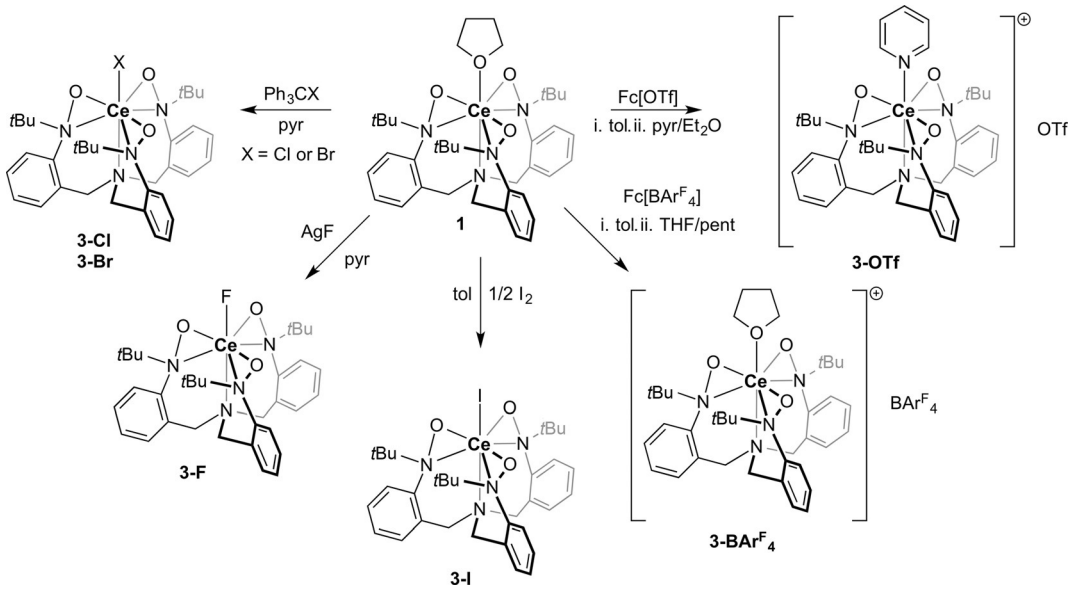

Scheme 2. Schematic of the redox chemistry performed on **1** to form the series of **3-X** complexes, in which **X** = **BAr$^F{}_4$**, **OTf**, **F**, **Cl**, **Br**, and **I**.

to that of 1.433(2) Å for the N–O bonds found in **1**.[5b,14] The average Ce–$O_{nitroxide}$ and Ce–$N_{nitroxide}$ bond lengths of 2.156(5) and 2.493(6) Å, respectively, in **3-BAr$^F_4$** and 2.177(3) and 2.489(3) Å in **3-OTf** were approximately 0.10–0.14 Å shorter than those in **1** consistent with the smaller ionic radius of Ce^{IV} compared to Ce^{III}.[15] Lastly, the Ce–O_{thf} bond length of 2.507(4) Å in **3-BAr$^F_4$** and the Ce–N_{pyr} bond length of 2.645(3) Å in **3-OTf** were typical of neutral oxygen and nitrogen donors bound to a Ce^{IV} cation.[5a,g]

A space-fill diagram of **1** with the THF molecule removed indicated that the $TriNO_x^{3-}$ framework limited the central cerium cation to one open coordination site that we postulated would allow the formation of stable 1:1 adducts with anionic ligands upon oxidation. To test this hypothesis, we sought to synthesize the halide series, Ce($TriNO_x$)X, in which X = F^- (**3-F**), Cl^- (**3-Cl**), Br^- (**3-Br**), and I^- (**3-I**), using AgF, Ph_3CCl, Ph_3CBr, and I_2 as oxidants, respectively. Indeed, these reactions proceeded cleanly and in moderate to good yields to dark red brown products in pyridine solutions for **3-F**, **3-Cl**, and **3-Br**, and toluene solution for **3-I** (Scheme 2). To the best of our knowledge, this is only the second complete halide series reported for Ce^{IV} within a conserved ligand framework. The other reported halide series for Ce^{IV} is the CeX[$N(SiMe)_3$] system completed by us with the isolation of CeF[$N(SiMe)_3$].[12] The low solubility of these complexes in solution made growing diffraction quality crystals difficult.[16] However, crystals of **3-Cl** suitable for X-ray diffraction analysis could be isolated by layering Et_2O onto a saturated pyridine solution of the complex.

Figure 3 shows the thermal ellipsoid plot of **3-Cl**. Again, the structural metrics were consistent with a central Ce^{IV} cation

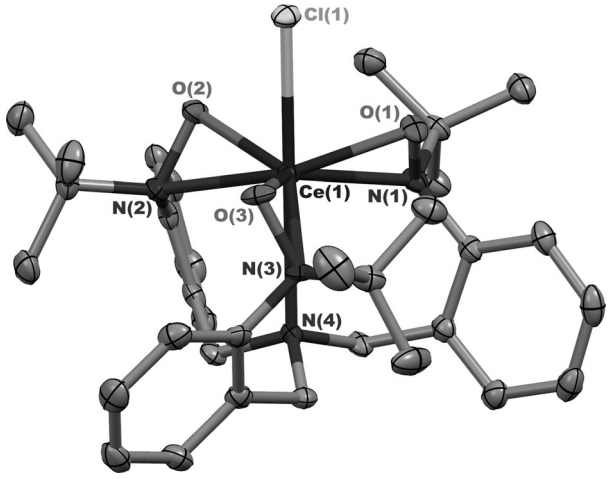

Figure 3. Thermal ellipsoid plot of **3-Cl**. Hydrogen atoms are omitted for clarity. Selected bond lengths [Å]: Ce(1)–O(1) 2.163(2), Ce(1)–O(2) 2.171(2), Ce(1)–O(3) 2.174(2), Ce(1)–N(1) 2.548(3), Ce(1)–N(2) 2.527(3), Ce(1)–N(3) 2.519(3), Ce(1)–Cl(1) 2.7436(8).

(Table 2). The Ce–Cl bond length of 2.7436(8) Å was significantly longer than that of 2.597(2) Å found in CeCl[$N(SiMe_3)_2]_3$ indicative of the larger steric demand of the $TriNO_x^{3-}$ ligand.[17] However, the Ce–Cl bond length in **3-Cl** was significantly shorter than that of 3.0080(3) Å in the known [{Ce(NN'_3)}$_2$(μ-Cl)], in which NN'_3 = [$N(CH_2CH_2N(SiMe_2tBu)]^{3-}$, due to the bridging mode of the chloride ligand between the $Ce^{III/IV}$ sites in the latter.[6a]

Table 2. Bond metrics for **1**, **3-BAr$^F_4$**, **3-OTf**, and **3-Cl**.

	1	3-BAr$^F_4$	3-OTf	3-Cl
N–O	1.433(2)	1.418(8)–1.436(7)	1.431(4)–1.435(4)	1.425(3)–1.436(3)
(Ce–$O_{nitroxide}$)$_{av}$	2.2921(18)	2.156(5)	2.177(3)	2.169(2)
(Ce–$N_{nitroxide}$)$_{av}$	2.581(2)	2.493(6)	2.489(3)	2.531(3)
Ce–X[a]	2.577(6)	2.507(4)	2.645(3)	2.7436(8)

[a] X = O_{thf} for **1** and **3-BAr$^F_4$**, N_{pyr} for **3-OTf**, and Cl^- for **3-Cl**.

The 4+ oxidation state of cerium in **3-Cl** was confirmed by Ce L_{III}-edge X-ray absorption spectroscopy. Figure 4 shows the

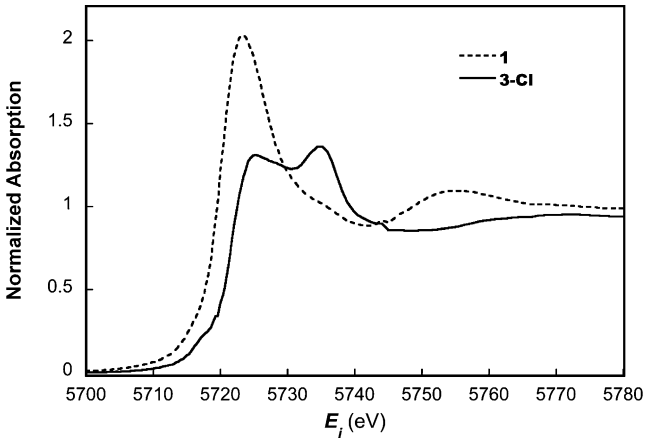

Figure 4. Overlay of the Ce L_{III}-edge XAS spectra of **1** and **3-Cl**.

near-edge regions of the XAS spectra of **1** and **3-Cl**. The spectrum of **3-Cl** showed the two features indicative of the core-hole excitation from a central Ce^{IV} cation to final states $2\underline{p}4f^1\underline{L}5d^1$ and $2\underline{p}4f^05d^1$, in which $\underline{L}$ indicates a ligand hole. The data were compared to the spectrum of **1**, which showed only one feature indicative of the core-hole excitation from a central Ce^{III} cation to final state $2\underline{p}4f^1\underline{L}5d^1$.[18]

Interestingly, the ^{1}H NMR spectrum of **3-Br** in deuterated pyridine showed two Ce^{IV} species in solution in a 4:1 ratio by integration. To gain insight into the identities of these two species, **3-Br** was synthesized by an alternate route starting from the reported Ce^{IV} complex, CeBr[$N(SiMe_3)_2]_3$,[5f] and protonated H_3TriNO_x. The ^{1}H NMR spectrum of the isolated dark red brown powder from this protonolysis reaction was identical to that of **3-Br** synthesized by using Ph_3CBr, with the same two Ce^{IV} species in solution again in a 4:1 ratio by integration. These data indicated that the presence of two Ce^{IV} species was characteristic of the solution chemistry of the **3-Br** product and not due to different reaction pathways occurring during the oxidation process. Based on these results, the two Ce^{IV} species were assigned as Ce($TriNO_x$)Br and [Ce($TriNO_x$)]Br, with inner- and outer-sphere bromide ions, respectively. This assignment was supported by electrochemistry experiments and corroborated

by more detailed analysis of the ^{1}H NMR spectroscopic data (see below).

An analogous route to the formation of **3-F** from **1** was not readily available. However, a titanium fluoride complex supported by the $TriNO_x^{3-}$ ligand framework was recently reported by us through reaction of [Ti($TriNO_x$)]Cl with AgF.[19] Reduction of Ag^+ by **1** to Ag^0 ($E_{1/2}$ $Ag^{+/0}$ = 0.65 V vs. Fc/Fc^+ in CH_2Cl_2) would also be thermodynamically favorable.[20] Therefore, AgF was expected to act as both an oxidant and fluoride-transfer reagent toward **1**. Indeed, reaction of **1** with AgF in pyridine led to the clean formation of Ag^0 and **3-F**.

The final complex of the series, **3-I**, was synthesized from **1** in an analogous manner as **3-F** using AgI as the oxidant. However, our preferred method was the synthesis of **3-I** in toluene using 0.5 equivalents of I_2 as the oxidant. This led to the precipitation of **3-I**, which was easily isolated as an analytically pure dark brown powder.

Solution electrochemistry

Solution electrochemistry experiments were performed on the series of **3-X**, in which **X** = **BAr^F_4**, **OTf**, **F**, **Cl**, **Br**, and **I**, in 0.10 M [^{n}Pr$_4$N][BAr^F_4] dichloromethane solutions. Figure 5 shows the metal-based $Ce^{III/IV}$ redox couples for the series of complexes.

The cyclic voltammograms of **3-BAr^F_4** and **3-OTf** exhibited metal-based features with $E_{pa} = -0.86$ V and $E_{pc} = -1.04$ V versus Fc/Fc^+, which were at similar potentials to the $Ce^{III/IV}$ feature in **1**, consistent with their solid-state structures of having non-coordinating, outer-sphere anions.

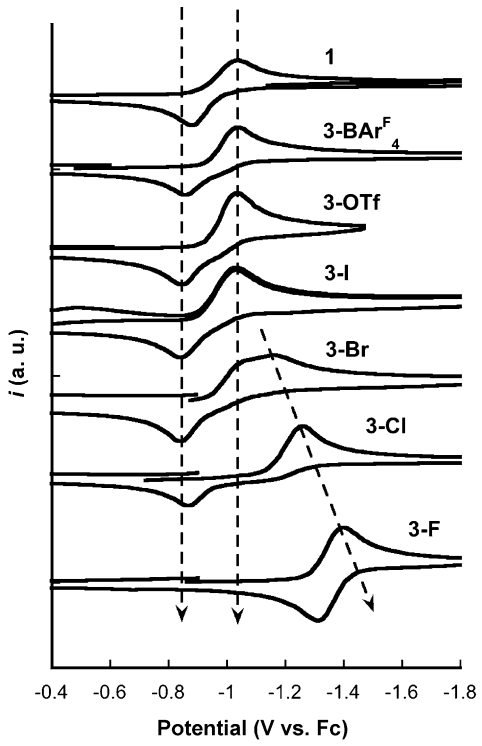

Figure 5. Metal-based $Ce^{IV/II}$ redox regions of the cyclic voltammograms for **1** and **3-X** collected at a scan rate of 100 mV s^{-1}.

It is noteworthy that the cyclic voltammogram of **3-Br** exhibited two separate reduction features consistent with the ^{1}H NMR spectrum of the complex, which showed two Ce^{IV} species in solution. The first reduction feature occurred with an E_{pc} of approximately −1.04 V, which was similar to those observed in **1**, **3-BAr^F_4**, and **3-OTf**, supporting the assignment of this feature to the reduction of the [Ce($TriNO_x$)]Br species with an outer-sphere bromide ion. The second reduction feature occurred with an $E_{pc} = -1.16$ V, which was assigned as the reduction of the Ce($TriNO_x$)Br species, with an inner sphere bromide ion. Despite the presence of two species in solutions of **3-Br**, only one return metal-based oxidation feature with $E_{pa} = -0.85$ V was observed in the cyclic voltammogram. Given the similarity of this feature to the return oxidation waves for **1**, **3-BAr^F_4**, and **3-OTf**, this suggested that upon reduction to Ce^{III}, the bromide ion dissociated from the $[Ce^{III}(TriNO_x)Br]^-$ species on the electrochemical timescale.

The cyclic voltammogram of **3-Cl** was similar to that of **3-Br** except that only one reduction feature with $E_{pc} = -1.26$ V was observed. This observation was consistent with effectively all of the chloride ligand being bound to the cerium cation in solution. The shift of 100 mV towards more negative potentials between the E_{pc} of **3-Cl** and that of **3-Br** was a result of increased stabilization of the 4+ oxidation state of the central-metal cation by Cl^- compared to Br^- (Figure 5). However, the return oxidation feature occurred with $E_{pa} = -0.87$ V, which indicated that upon reduction of the metal center, the chloride ion dissociated from the central Ce^{III} cation similar to the case of the $[Ce^{III}(TriNO_x)Br]^-$ species in solutions of **3-Br**.

Unlike in the cyclic voltammograms of **3-Cl** and **3-Br**, the metal-based feature in the cyclic voltammogram of **3-F** was more reversible ($E_{pa} = -1.31$ V, $E_{pc} = -1.40$ V vs. Fc/Fc^+). The 140 mV shift towards more negative potentials between the E_{pc} of **3-F** and that of **3-Cl** indicated that F^- more effectively stabilized the 4+ oxidation state of Ce than Cl^-. However, the large shift in potential of 440 mV towards more negative potentials between the E_{pa} of **3-F** and that of **3-Cl**, and the reversibility of the wave for **3-F**, indicated that the fluoride ion remained bound to the reduced $[Ce^{III}(TriNO_x)F]^-$ species. Based on the similarity of the metal-based wave in the CV of **3-I** to that of **1**, **3-BAr^F_4**, and **3-OTf**, the solution structure of **3-I** was assigned as [Ce($TriNO_x$)]I with completely outer-sphere iodide. These results were corroborated through analysis of the ^{1}H NMR spectroscopic data for **3-F**, **3-Cl**, **3-Br**, and **3-I** (see below).

A similar trend in the potential of the $Ce^{III/IV}$ redox couple was observed in the electrochemistry of the related CeX[N(-$SiMe_3)_2]_3$ halide series. There, the addition of a Br^- ligand to the central cerium cation shifted the measured reduction potential by 0.66 V to more negative potentials, whereas replacing the Br^- with a Cl^- had no effect on the position of the of the measured redox potential. This potential was shifted by a further 0.25 V through the coordination of an F^- ligand. However, the peak separations of the CeBr[$N(SiMe_3)_2]_3$ and CeCl[$N(SiMe_3)_2]_3$ complexes were significantly smaller than the related **3-Br** and **3-Cl** complexes due to the dissociation of halide ligands upon reduction of the latter. The peak separa-

tion of the **3-F** complex, in which fluoride coordination was conserved during the redox cycling, was significantly smaller than that of the $CeF[N(SiMe_3)_2]_3$ complex, suggesting fast electron-transfer (ET) kinetics in the redox cycling of **3-F**.

^{1}H NMR spectroscopy

The solution structures of **3-F**, **3-Cl**, **3-Br**, and **3-I** were studied in deuterated pyridine by using ^{1}H NMR spectroscopy. As shown in Figure 6, all the complexes displayed characteristic

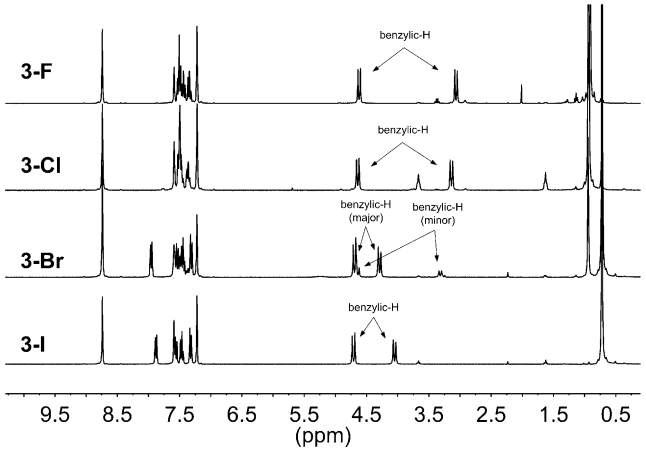

Figure 6. ^{1}H NMR (in $[D_5]$pyr) spectral overlay.

diamagnetic ^{1}H NMR spectra with resonances appearing in the $\delta = 0$–10 ppm range. The presence of diastereotopic benzylic resonances between 2.5–5.0 ppm was indicative of coordination of $TriNO_x^{3-}$ to the central Ce cation. However, subtle differences in the ^{1}H NMR spectra were observed. Both **3-F** and **3-Cl** have aromatic resonances between $\delta = 7.5$ and 7.3 ppm, diastereotopic benzylic proton resonances at approximately 4.5 and 3 ppm for both species ($\Delta\delta_{benzylH} > 1$ ppm), and *tert*-butyl resonances at around 0.90 ppm. Based on solid-state structural determination of **3-Cl** and the solution electrochemical data across the series, these spectral signatures were attributed to species with coordinated halides.

In contrast, the aromatic resonances of **3-I** were more diffuse and appeared as far up field as 7.9 ppm. Furthermore, the diastereotopic benzylic proton resonances were closer together at 4.7 and 4.0 ppm ($\Delta\delta_{benzylH} = 0.7$ ppm), and the *tert*-butyl resonance was shifted upfield by 0.2 to 0.7 ppm. These spectral signatures were assigned to the species with outer-sphere halides. The NMR spectroscopy characteristics are similar to what was observed in the case of $Ti(TriNO_x)F$, in which a coordinated fluoride ligand compared to an outer-sphere chloride ligand resulted in the appearance of an aromatic resonance downfield at 7.89 ppm, as well as diastereotopic benzylic resonances with a smaller shift: $\Delta\delta_{benzylH}$ ($\Delta\delta_{benzylH} = 1.56$ for $Ti(TriNO_x)F$; $\Delta\delta_{benzylH} = 0.48$ for $[Ti(TriNO_x)]Cl$).[19]

As mentioned above, **3-Br** was unique in that both species were present in solution, as indicated by the presence of two sets of diastereotopic benzylic proton resonances in a 4:1 ratio by integration. The major species had an aromatic resonance at 7.95 ppm, diastereotopic benzylic proton resonances with a $\Delta\delta_{benzylH}$ of 0.4 ppm, and a *tert*-butyl resonance at 0.72 ppm. The minor species exhibited aromatic resonances between 7–7.5 ppm, diastereotopic benzylic proton resonances with a $\Delta\delta_{benzylH}$ of 1.3 ppm, and a *tert*-butyl resonance at 0.94 ppm. These spectral characteristics supported the assignment of the major species as $[Ce(TriNO_x)]Br$ with an outer-sphere bromide and the minor species as $Ce(TriNO_x)Br$ with an inner-sphere bromide ligand.

DFT calculations

Cerium pyridyl nitroxide systems reported recently by us showed strong stability of the 4+ oxidation state of Ce due to symmetry allowed donation from the N–O π^* orbitals into the Ce $4f_{z(x^2-y^2)}$ as a result of the D_{2d} complex symmetry,[10] and Kozimor and co-workers recently describe metal–ligand covalency for a Ce^{IV} chloride complex using chlorine K-edge XAS spectroscopy.[21] We hypothesized that symmetry allowed donation from $TriNO_x^{3-}$ into the $4f_{y(3x^2-y^2)}$ orbital of Ce as a result of the C_3 complex symmetry was similarly lending structural stability to these complexes.

The frontier molecular orbitals of $[Ce(TriNOx)thf]^+$ ($[\mathbf{1}]^+$), the cationic portion of **3-BAr$^F_4$**, were compared with those of **1**. Indeed, the in-phase interaction between the oxygen 2p orbitals of $TriNO_x^{3-}$ and the Ce $4f_{y(3x^2-y^2)}$ orbital was observed in the HOMO−12 of $[\mathbf{1}]^+$. The corresponding out-of-phase interaction was observed in the LUMO+6. The main interaction between the orbitals of $TriNO_x^{3-}$ and those of the central cerium cation in $[\mathbf{1}]^+$, however, was observed in the HOMO with head-on overlap of the N–O π^* orbitals with a linear combination of the Ce $4f_{z^3}$ and Ce $4f_{x(x^2-3y^2)}$ orbitals. The corresponding antibonding interaction of these orbitals was observed in the LUMO+3 (Figure 7). In contrast, the occupied frontier MOs of **1** contained less Ce 4f character, whereas the frontier unoccupied MOs of **1** contained less ligand character.

To corroborate these findings, population analyses on **1** and $[\mathbf{1}]^+$ were performed. Upon oxidation of the central metal cation from Ce^{III} to Ce^{IV}, there was a marginal increase in the natural charge on cerium, q_{Ce}, from 1.78 to 1.90, as was expected for an increase in formal oxidation state. However, the natural charge to formal charge ratio decreased from 0.593 in **1** to 0.475 in $[\mathbf{1}]^+$. As shown in Table 3, this decrease was a result of increased donation of the ligand electron density into the unfilled 4f, 5d, and 6s orbitals on the cerium cation.

Population and Mayer bond order (MBO) analyses were also performed on geometry-optimized structures of **3-F**, **3-Cl**, **3-Br**, and **3-I** to probe the ionicity and strength of the metal–halide bond. The metrics suggested that the ionicity of the Ce–halide bond generally decreased upon traversing the series towards the heavier halides, as was indicated by the smaller positive natural charge on cerium and the smaller negative natural charge on the X ligand. However, the metal–iodide bond was calculated to be more ionic than the metal–bromide bond and comparable to that of the metal–chloride bond. Similarly, there was a general decrease in the strength of the Ce–X bond

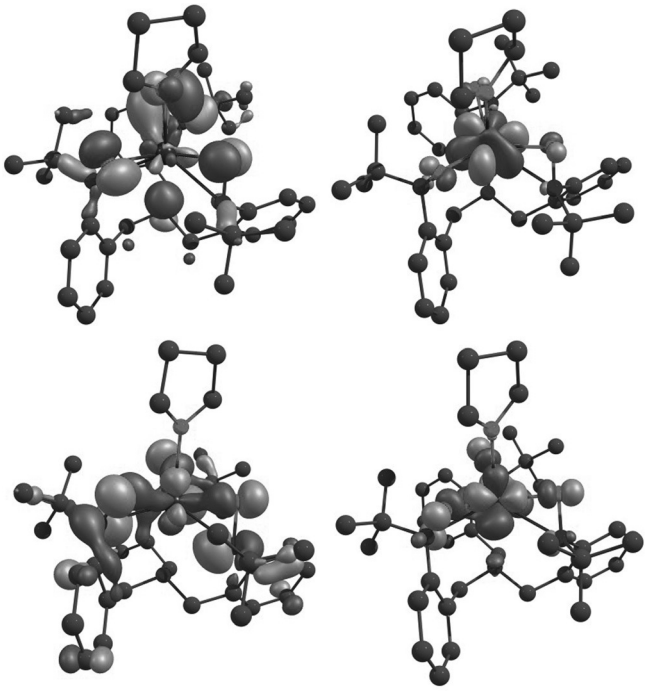

Figure 7. HOMO−12 (top left), LUMO+6 (top right), HOMO (bottom left), and LUMO+3 (bottom right) of $[Ce(TriNOx)thf]^+$ ($[1]^+$), the cationic portion of **3-BAr$^F_4$**.

Table 3. Natural charges (q_{Ce} and q_X), natural populations (6s, 5d, and 4f), Mayer bond orders (MBOs), and theoretical formal shortness ratios (FSR) for **1**, $[1]^+$, **3-F**, **3-Cl**, **3-Br**, and **3-I**.

	q_{Ce}	q_X	Ce 6s	5d	4f	MBO Ce–X	FSR[a]
1	1.78	−0.60	0.11	0.83	0.17	0.202	
$[1]^+$	1.90	−0.61	0.13	1.01	0.87	0.255	
3-F	1.89	−0.53	0.12	1.04	0.85	1.044	0.892
3-Cl	1.71	−0.48	0.15	1.17	0.88	0.973	0.946
3-Br	1.66	−0.44	0.17	1.20	0.88	0.940	0.948
3-I	1.68	−0.49	0.18	1.18	0.88	0.870	0.988

[a] FSR = (calculated bond length$_{Ce-X}$)/(ionic radius$_{Ce}^{IV}$ + ionic radius$_X^-$).

across the series, as was indicated by the decrease in MBO from 1.044 for **3-F** to 0.870 for **3-I**. This is consistent with the solution chemistry of these species in coordinating solvents, such as pyridine, in which solvent molecules competed with the heavier halides for metal ligation.

Another useful metric for determining the strength of the metal–halide interaction is the theoretical formal shortness ratio (FSR) of the metal–halide bond. These were calculated for the series of Ce–halide complexes using the determined Ce–X bond length from the gas-phase optimized structures and the tabulated Shannon radii for Ce^{4+} and X^- ions. Values significantly less than one indicate stronger interactions between metal and halide ligand. As shown in Table 3, the theoretical FSR of the Ce–X bond increased significantly from 0.892 in **3-F** to 0.988 in **3-I**. This trend is consistent with experiment, as well as the findings from the MBO analysis.

These results are in contrast with those obtained from calculations on the $CeX[N(SiMe_3)_2]_3$ system. Similar to the **3-X** series, the ionicity of the metal–halide bonds in the $CeX[N(SiMe_3)_2]_3$ series generally decreased with coordination of the heavier halides. However, unlike in the **3-X** series, the calculated MBO of the Ce–X bond in the $CeX[N(SiMe_3)_2]_3$ system trended upward with coordination of the heavier halides.

Conclusion

The Ce^{III} precursor **1** was successfully synthesized and used as a starting material for controlled redox chemistry at the central cerium cation. Detailed solution electrochemistry experiments showed that the tripodal nitroxide environment of $TriNO_x^{3-}$ provided significant stabilization of the Ce^{IV} oxidation state, as was indicated by the measured $Ce^{III/IV}$ redox potential of −0.96 V versus Fc/Fc^+. The electron-rich and sterically protected environment imposed by the $TriNO_x^{3-}$ framework allowed the isolation and characterization of the stable cationic Ce^{IV} complexes, **3-BAr$^F_4$** and **3-OTf**. Due to the strong Lewis acidity of the Ce^{IV} cation, these types of complexes are quite rare. However, the $TriNO_x^{3-}$ framework was sufficiently bulky and electron rich to mitigate the high Lewis acidity of Ce^{IV}.

The complete halide series, **3-X**, in which **X** = **F**, **Cl**, **Br**, and **I**, was also synthesized. Herein, the bulky $TriNO_x^{3-}$ framework caused diverse solution behavior within the series. When the size of the X^- ligand increased, we observed increased concentrations of $[Ce(TriNO_x)]X$ species, with outer-sphere halides in solution. We are interested in exploring the use of Ce^{IV} supported by $TriNO_x^{3-}$-type frameworks in Lewis acid catalysis, which would require binding and activation of substrate through polarization of the Ce–substrate bond. Further modification of the nitrogen R groups is, therefore, warranted to accommodate larger anionic ligands in the cleft and to prevent the formation of outer-sphere anions.

Experimental Section

General methods

Unless otherwise noted, all reactions and manipulations were performed under an inert atmosphere (N_2) using standard Schlenk techniques or in a drybox equipped with a molecular sieves 13X/Q5 Cu-0226S catalyst purifier system. Glassware was oven dried for at least three hours at 150 °C prior to use. ^1H and $^{19}F\{^1H\}$ NMR spectra were obtained on a Bruker DMX-300 Fourier transform NMR spectrometer at 300 MHz and 282.2 MHz, respectively. $^{13}C(^1H)$ NMR spectra were obtained on a Bruker DRX-500 Fourier transform NMR spectrometer or a Bruker AVIII 500 Fourier transform NMR spectrometer equipped with a cryogenic probe at 125.7 MHz. Chemical shifts were recorded in units of parts per million downfield from residual proteo solvent for ^1H NMR, characteristic solvent peaks for ^{13}C NMR, or relative to an external $CFCl_3$ reference (0 ppm). Elemental analyses were performed either at the University of California, Berkeley, Microanalytical Facility using a PerkinElmer Series II 2400 CHNS analyzer or at Complete Analysis Laboratories, Inc. using a Carlo Erba EA 1108 analyzer.

Materials

Tetrahydrofuran, dimethoxyethane, diethyl ether, dichloromethane, toluene, hexanes, and pentane were purchased from Fisher Scientific. All solvents were sparged for 20 min with dry N_2 and dried using a commercial two-column solvent-purification system comprising columns packed with Q5 reactant and neutral alumina respectively (for hexanes and pentane), or two columns of neutral alumina (for THF, Et_2O, and CH_2Cl_2). Deuterated solvents were purchased from Cambridge Isotope Laboratories, Inc. and stored over 4 Å molecular sieves prior to use. Cerium chloride (Strem), potassium bis(trimethylsilyl)amide (Sigma), silver triflate, trityl chloride, and trityl bromide were used as received. Iodine was sublimed prior to use. Fc[BAr^F_4],[22] Fc[OTf],[23] Ce[$N(SiMe_3)_2$]$_3$,[24] and [nPr$_4$N][B(3,5-$(CF_3)_2$-$C_6H_3)_4$][25] were synthesized according to literature procedures.

Electrochemistry

All experiments were performed under an inert atmosphere (N_2) in a drybox with electrochemical cells that consisted of a 4 mL vial, glassy carbon disk (3 mm diameter) working electrode, a platinum-wire counterelectrode, and a silver wire plated with AgCl as a quasi-reference electrode. The working electrode surfaces were polished prior to each set of experiments. Potentials recorded in CH_2Cl_2 were referenced versus ferrocene, which was added as an internal standard for calibration at the end of each run. Solutions employed during CV studies were approximately 3 mM in analyte and 100 mM in [nPr$_4$N][BAr^F_4]. All data were collected in a positive-feedback IR compensation mode. The CH_2Cl_2 solution cell resistances were measured prior to each run to insure resistances $\leq\approx$500 Ω.[25] Scan-rate dependences of 50–1000 mV s^{-1} were performed to determine electrochemical reversibility.

X-ray crystallography

X-ray intensity data were collected on a Bruker APEXII CCD area detector employing graphite-monochromated $Mo_{K\alpha}$ radiation (λ = 0.71073 Å) at a temperature of 143(1) K. In all cases, rotation frames were integrated using SAINT,[26] producing a listing of unaveraged F^2 and $\sigma(F^2)$ values, which were then passed to the SHELXTL[27] program package for further processing and structure solution. The intensity data were corrected for Lorentz and polarization effects and for absorption using TWINABS[28] or SADABS.[29] The structures were solved by direct methods (SHELXS-97).[30] Refinement was done by full-matrix least squares based on F^2 using SHELXL-97.[30] All reflections were used during refinements. Non-hydrogen atoms were refined anisotropically and hydrogen atoms were refined using a riding model.

X-ray absorption spectroscopy

Ce L_{III}-edge XANES data were collected at the Stanford Synchrotron Radiation Lightsource, beamline 11–2, using a Si 220 (ϕ = 0) double monochromator that was detuned to 20% to reduce harmonic contamination. The resulting data have an energy resolution limited by the broadening due to the $2p_{3/2}$ core-hole lifetime of 3.2 eV. Data were collected in transmission, using a CeO_2 reference to calibrate the energy scale, setting the first inflection point of the CeO_2 absorption to 5723 eV. A linear pre-edge background was subtracted, and the data were subsequently normalized at 5800 eV.

The samples were prepared for these experiments using procedures outlined previously.[31] In particular, each sample was ground into a powder, mixed with dry boron nitride as a diluent, and then packed into the slots of a machined aluminum sample holder in an N_2 atmosphere drybox. Aluminized mylar was affixed to the holder with an indium-wire seal. After packaging, the samples were transported in dry, nitrogen-filled containers to the beamline. Sample holders were quickly transferred to the vacuum chamber, exposing the sealed holders to air for less than thirty seconds before pumping out the chamber and collecting the data under vacuum. Compound **1** is extreme air sensitive and has easily identifiable spectral changes upon exposure. This sample served as a "canary" sample and was monitored to check for sample-holder integrity. Following measurement, no significant changes in the sample were observed.

Computational details

Gaussian 09, Revision D.01, was used in electronic structure calculations.[32] The B3LYP hybrid DFT method was employed, with a 28-electron small core pseudopotential on cerium with published segmented natural orbital basis set incorporating quasi-relativistic effects,[33] and the 6–31G* basis set on all other atoms.[34] No restraints were imposed other than spin. Frequency calculations were preformed to confirm the geometry was a minimum (no negative frequencies). NBO calculations were run using the NBO6 package.[35] Fragment orbital analysis was performed using the AOMix software.[36] Molecular orbitals were rendered with the ChemCraft v1.6 program.[37]

Synthetic details and characterization

Ce(TriNO$_x$)THF (**1**): Ce(TriNO$_x$)THF was synthesized by modifying a previously published procedure.[9] A THF solution of H_3TriNO$_x$ (0.26 g, 0.47 mmol, 1 equiv) was layered on a hexanes solution of Ce[$N(SiMe_3)_2$]$_3$ (0.30 g, 0.47 mmol, 1 equiv). The reaction was allowed to sit, undisturbed, at room temperature for 48 h. The resulting red orange crystals of **1** were collected, washed with THF, and dried under reduced pressure. Yield: 0.30 g (84%). ^{1}H NMR (500 MHz, [D_5]pyr): δ = 13.04 (d, J = 6.5 Hz, 3H) 8.39 (dd, J = 6.7, 6.5 Hz, 3H), 7.15 (dd, J = 7.2, 6.7 Hz, 3H), 4.58 (d, J = 7.2 Hz, 3H), 3.66 (m, 4H), 2.95 (s, 27H), −3.28 (s, 3H), −3.58 ppm (s, 3H); elemental analysis calcd for $C_{37}H_{53}N_4O_4Ce$ (M_w = 757.97 g mol^{-1}): C 58.63, H 7.05, N 7.39; found: C 58.88, H 7.05, N 7.56.

[Ce(TriNO$_x$)]$_2$ (**2**): [Ce(TriNO$_x$)]$_2$ was synthesized by modifying a previously published procedure.[9] Isolated **1** (0.088 g, 0.12 mmol, 1 equiv) was dissolved in toluene, and solvent was removed under reduced pressure. Yield: 0.083 g (92%). ^{1}H NMR (500 MHz, C_6D_6): δ = 30.31 (a.s., a.s. = apparent singlet, 2H), 16.76 (a.s., 2H), 13.87 (a.s., 2H), 10.65 (a.t., J = 7.2 Hz, 2H), 10.29 (a.s., 2H), 9.22 (d, J = 7.2 Hz, 2H), 6.76 (a.t., J = 7.2 Hz, 2H), 4.71 (br s, 18H), 2.06 (s, 2H), 1.38 (d, J = 5.5 Hz, 2H), 1.18 (s, 2H), 1.03 (s, 2H), 0.94 (a.t, J = 6.8 Hz, 2H), −0.08 (s, 18H), −0.79 (s, 2H), −2.46 (d, J = 7.2 Hz, 2H), −3.21 (a.s., 2H), −4.79 (s, 18H), −5.18 (s, 2H), −10.15 (a.s., 2H), −13.56 ppm (a.s., 2H); elemental analysis calcd for $C_{66}H_{90}N_8O_6Ce_2$·Et_2O (M_w = 1445.85 g mol^{-1}): C 58.15, H 6.97, N 7.75; found: C 58.13, H 6.89, N 7.77.

Ce(TriNO$_x$)F (**3-F**): To a pyridine solution of **1** (0.10 g, 0.13 mmol, 1 equiv) was added solid AgF (0.018 g, 0.15 mmol, 1.1 equiv), and the reaction was stirred in the dark for 6 h. The Ag^0 by-product was removed by filtration through a coarse porosity fritted filter and the pyridine filtrate was collected. Volatiles were removed under reduced pressure, and the resulting dark red brown powder was washed with minimal diethyl either and dried. Isolated yield: 0.026 g (28%). ^{1}H NMR (300 MHz, [D_5]pyr): δ = 7.56–7.47 (overlap 6H), 7.43 (ddd, J = 7.7, 7.5, 1.8 Hz, 3H), 7.34 (ddd, J = 7.6, 7.5, 1.5 Hz, 3H), 4.62 (d, J = 11.9 Hz, 3H), 3.06 (d, J = 11.9 Hz, 3H),

0.091 ppm (s, 27H); ^{13}C NMR (125.7 MHz, [D$_5$]pyr): δ = 149.6, 133.3, 133.0, 130.1, 129.6, 127.9, 65.2, 62.1, 26.5; ^{19}F NMR (282.2 MHz, [D$_5$]pyr): δ = 219.1 ppm; elemental analysis calcd for $C_{33}H_{45}N_4O_3CeF$ (M_w = 704.86 g mol^{-1}): C 56.23, H 6.44, N 7.95; found: C 55.99, H 6.54, N 8.09.

Ce(TriNO$_x$)Cl (**3-Cl**): To a pyridine solution of **1** (0.10 g, 0.13 mmol, 1 equiv) was added solid Ph_3CCl (0.056 g, 0.20 mmol, 1.5 equiv) and the reaction was stirred for 3 h. Volatiles were removed under reduced pressure, and the resulting dark red brown solid was washed with Et_2O and dried. X-ray quality crystals were obtained by vapor diffusion of diethyl ether into a saturated pyridine solution of **3-Cl**. Yield: 0.079 g (84%). ^{1}H NMR (300 MHz, [D$_5$]pyr): δ = 7.56–7.42 (overlap, 9H), 7.36 (a.td., a.td. = apparent triplet of doublets, J = 7.1, 2.1 Hz, 3H), 4.64 (d, J = 12.0 Hz, 3H), 3.14 (d, J = 12.0 Hz, 3H), 0.94 ppm (s, 27H); ^{13}C NMR (125.7 MHz, [D$_5$]pyr): δ = 133.1, 133.0, 130.3, 129.9, 128.4, 66.3, 62.0, 26.8; elemental analysis calcd for $C_{33}H_{45}N_4O_3CeCl$ (M_w = 721.31 g mol^{-1}): C 54.95, H 6.29, N 7.77; found: C 54.57, H 6.57, N 7.76.

Ce(TriNO$_x$)Br (**3-Br**): *Method A:* Ce(TriNO$_x$)Br was synthesized in a similar manner to Ce(TriNO$_x$)Cl, except Ph_3CBr was used as the oxidant. To a pyridine solution of **1** (0.074 g, 0.098 mmol, 1 equiv) was added solid Ph_3CBr (0.047 g, 0.15 mmol, 1.5 equiv), and the reaction was stirred for 3 h. The reaction mixture was filtered, and volatiles were removed under reduced pressure. The resulting dark red brown solid was washed with Et_2O and dried. Yield: 0.059 g (79%). *Method B:* To a THF solution of H_3TriNO_x (0.060 g, 0.11 mmol, 1 equiv) was then added a THF solution of freshly prepared $CeBr[N(SiMe_3)_2]_3$ (0.077 g, 0.11 mmol, 1 equiv), and the reaction was allowed to react for 3 h, after which a dark red brown solid precipitated. This solid was isolated on a medium-porosity fritted filter, washed with Et_2O, and dried under reduced pressure. Yield: 0.030 g (36%). ^{1}H NMR (300 MHz, [D$_5$]pyr): δ (major species, 80%) = 7.95 (d, J = 7.6 Hz, 3H), 7.59–7.27 (overlap, 9H), 4.69 (d, J = 12.4 Hz, 3H), 4.29 (d, J = 12.4 Hz, 3H), 0.72 ppm (s, 27H); (minor species, 20%) 7.59–7.27 (overlap, 12H), 4.64 (d, J = 12.1 Hz, 3H), 3.32 (d, J = 12.1 Hz, 3H), 0.94 ppm (s, 27H); ^{13}C NMR (125.7 MHz, [D$_5$]pyr): δ (major species) = 146.9, 134.4, 132.9, 130.7, 130.5, 129.6, 66.9, 59.7, 26.9 ppm; (minor species) 148.7, 133.3, 133.1, 130.3, 130.0, 128.5, 66.6, 61.6, 26.9 ppm (overlap); elemental analysis calcd for $C_{33}H_{45}N_4O_3CeBr$ (M_w = 765.77 g mol^{-1}): C 51.76, H 5.92, N 7.32; found C 51.55, H 5.82, N 7.15.

Ce(TriNO$_x$)I (**3-I**): To a toluene solution of **1** (0.20 g, 0.26 mmol, 1 equiv) was added solid I_2 (0.040 g, 0.13 mmol, 0.6 equiv) causing the immediate precipitation of a dark red brown powder. The reaction was stirred for 6 h. The dark red brown powder was isolated on a medium-porosity fritted filter, washed with Et_2O, and dried under reduced pressure. Yield: 0.17 g (79%). ^{1}H NMR (300 MHz, [D$_5$]pyr): δ = 7.88 (dd, J = 7.5, 1.7 Hz, 3H), 7.56 (ddd, J = 8.0, 7.7, 1.7 Hz, 3H), 7.46 (ddd, J = 7.7, 7.5, 1.4 Hz, 3H), 7.32 (dd, J = 8.0, 1.4 Hz), 4.71 (d, J = 12.5 Hz, 3H), 4.05 (d, J = 12.5 Hz), 0.72 ppm (s, 27H); ^{13}C NMR (125.7 MHz, [D$_5$]pyr): δ = 146.9, 134.2, 132.6, 130.9, 130.6, 129.7, 67.0, 60.0, 26.9 ppm; elemental analysis calcd for $C_{33}H_{45}N_4O_3CeI$ (M_w = 812.77 g mol^{-1}): C 48.77, H 5.58, N 6.89; found: C 48.63, H 5.37, N 6.79.

[Ce(TriNO$_x$)THF][BAr$^F_4$] (**3-BAr$^F_4$**): To a toluene solution of **1** (0.30 g, 0.39 mmol, 1 equiv) was added Fc[BAr$^F_4$] (0.41 g, 0.39 mmol, 1 equiv), and the reaction was stirred for 14 h. Volatiles were removed under reduced pressure, and the resulting dark red brown powder was rinsed with hexanes and recrystallized from vapor diffusion of pentane into a saturated THF solution. Yield: 0.39 g (61%). ^{1}H NMR (300 MHz, [D$_5$]pyr): δ = 8.43 (m, 8H), 7.84 (br s, 4H), 7.69–7.57 (overlap, 6H), 7.49 (a.td., J = 7.4, 1.2 Hz, 3H), 7.37 (dd, J = 8.0, 0.8 Hz, 3H), 4.75 (d, J = 12.5 Hz, 3H), 3.67 (m, 4H), 3.40 (d, J = 12.5 Hz, 3H), 1.63 (m, 4H), 0.74 ppm (s, 27H); ^{13}C NMR (125.7 MHz, [D$_5$]pyr): δ = 163.1 (q, ^1J(^{11}B,^{13}C) = 49 Hz), 146.9, 133.9, 132.1, 131.1, 130.8, 130.3 (qq, ^2J(^{19}F,^{13}C) = 31, ^4J(^{19}F,^{13}C) = 3 Hz), 129.8, 125.5 (q, ^1J(^{19}F,^{13}C) = 273 Hz), 118.7 (sept, ^3J(^{19}F,^{13}C) = 4 Hz), 68.3, 67.1, 60.9, 26.8, 26.3 ppm; ^{19}F NMR (282.2 MHz, [D$_5$]pyr): δ = −62.1; elemental analysis calcd for $C_{69}H_{65}N_4O_4F_{24}BCe$ (M_w = 1621.19 g mol^{-1}): C 51.12, H 4.04, N 3.46; found: C 50.87, H 4.14, N 3.24.

[Ce(TriNO$_x$)pyr][OTf] (**3-OTf**): To a toluene solution of **1** (0.057 g, 0.075 mmol, 1 equiv) was added solid FcOTf (0.025, 0.075 mmol, 1 equiv), and the reaction was stirred for 5 h. The resulting dark red brown powder was isolated on a medium-porosity fritted filter and rinsed with Et_2O. Crystals of **3-OTf** suitable for X-ray diffraction analysis were grown for vapor diffusion of Et_2O into a saturated pyridine solution. Yield: 0.040 g (58%). ^{1}H NMR (300 MHz, [D$_5$]pyr): δ = 7.79 (dd, J = 7.4, 1.7 Hz, 3H), 7.57 (ddd, J = 8.1, 7.4, 1.7 Hz, 3H), 7.48 (ddd, J = 7.4, 7.4, 1.4 Hz, 3H), 7.33 (dd, J = 8.1, 1.4 Hz, 3H), 4.73 (d, J = 12.5 Hz, 3H), 3.69 (d, J = 12.5 Hz, 3H), 0.72 ppm (s, 27H); ^{13}C NMR (125.7 MHz, [D$_5$]pyr): δ = 146.8, 134.1, 132.4, 130.9, 130.7, 129.8, 67.0, 60.4, 26.9 ppm; ^{19}F NMR (282.2 MHz, [D$_5$]pyr): δ = −77.2 ppm; elemental analysis calcd for $C_{39}H_{50}N_5O_6F_3SCe{\cdot}0.5pyr$ (M_w = 953.58 g mol^{-1}): C 52.27, H 5.55, N 8.08; found: C 52.22, H 5.62, N 7.96.

Acknowledgements

E.J.S. acknowledges the U.S. Department of Energy, Office of Science, Early Career Research Program (Grant DE-SC0006518), the Research Corporation for Science Advancement (Cottrell Scholar Award to E.J.S.), and the University of Pennsylvania for financial support of this work. This work used the Extreme Science and Engineering Discovery Environment (XSEDE), which is supported by the National Science Foundation Grant ACI-1053575. Portions of this work were supported by the Director, Office of Science (OS), Office of Basic Energy Sciences, of the U.S. Department of Energy (DOE) under Contract No. DE-AC-02-05CH11231 and were carried out at SSRL, a Directorate of SLAC National Accelerator Laboratory and an OS user facility operated for the DOE OS by Stanford University.

Keywords: cerium · density functional calculations · electrochemistry · nitroxides · redox chemistry

[1] N. A. Piro, J. R. Robinson, P. J. Walsh, E. J. Schelter, *Coord. Chem. Rev.* **2014**, *260*, 21–36.

[2] a) S. R. Sofen, S. R. Cooper, K. N. Raymond, *Inorg. Chem.* **1979**, *18*, 1611–1616; b) V. Nair, A. Deepthi, *Chem. Rev.* **2007**, *107*, 1862–1891.

[3] a) E. Mamontov, T. Egami, *J. Phys. Chem. Solids* **2000**, *61*, 1345–1356; b) D. Hong, M. Murakami, Y. Yamada, S. Fukuzumi, *Energy Environ. Sci.* **2012**, *5*, 5708–5716; c) D. J. Wasylenko, C. Ganesamoorthy, M. A. Henderson, C. P. Berlinguette, *Inorg. Chem.* **2011**, *50*, 3662–3672.

[4] C. K. Gupta, N. Krishnamurthy, *Int. Mater. Rev.* **1992**, *37*, 197–248.

[5] a) B. D. Mahoney, N. A. Piro, P. J. Carroll, E. J. Schelter, *Inorg. Chem.* **2013**, *52*, 5970–5977; b) J. A. Bogart, A. J. Lewis, M. A. Boreen, H. B. Lee, S. A. Medling, P. J. Carroll, C. H. Booth, E. J. Schelter, *Inorg. Chem.* **2015**, *54*, 2830–2837; c) J. R. Robinson, P. J. Carroll, P. J. Walsh, E. J. Schelter, *Angew. Chem. Int. Ed.* **2012**, *51*, 10159–10163; *Angew. Chem.* **2012**, *124*, 10306–10310; d) J. R. Robinson, C. H. Booth, P. J. Carroll, P. J. Walsh, E. J. Schelter, *Chem. Eur. J.* **2013**, *19*, 5996–6004; e) H. B. Lee, J. A. Bogart, P. J. Carroll, E. J. Schelter, *Chem. Commun.* **2014**, *50*, 5361–5363; f) U. J. Williams, P. J. Carroll, E. J. Schelter, *Inorg. Chem.* **2014**, *53*, 6338–6345; g) U. J. Williams, D. Schneider, W. L. Dorfner, C. Maichle-Mossmer, P. J. Carroll, R. Anwander, E. J. Schelter, *Dalton Trans.* **2014**, *43*, 16197–

16206; h) D. Werner, G. B. Deacon, P. C. Junk, R. Anwander, *Chem. Eur. J.* **2014**, *20*, 4426 – 4438; i) D. Schneider, T. Spallek, C. Maichle-Mossmer, K. W. Tornroos, R. Anwander, *Chem. Commun.* **2014**, *50*, 14763 – 14766; j) A. R. Crozier, C. Schadle, C. Maichle-Mossmer, K. W. Tornroos, R. Anwander, *Dalton Trans.* **2013**, *42*, 5491 – 5499; k) A. R. Crozier, A. M. Bienfait, C. Maichle-Mossmer, K. W. Tornroos, R. Anwander, *Chem. Commun.* **2013**, *49*, 87 – 89; l) P. Dröse, A. R. Crozier, S. Lashkari, J. Gottfriedsen, S. Blaurock, C. G. Hrib, C. Maichle-Mössmer, C. Schädle, R. Anwander, F. T. Edelmann, *J. Am. Chem. Soc.* **2010**, *132*, 14046 – 14047.

[6] a) C. Morton, N. W. Alcock, M. R. Lees, I. J. Munslow, C. J. Sanders, P. Scott, *J. Am. Chem. Soc.* **1999**, *121*, 11255 – 11256; b) P. Dröse, J. Gottfriedsen, *Z. Anorg. Allg. Chem.* **2008**, *634*, 87 – 90.

[7] a) L. H. Gade, *Acc. Chem. Res.* **2002**, *35*, 575 – 582; b) K. M. Wampler, R. R. Schrock, *Inorg. Chem.* **2007**, *46*, 8463 – 8465; c) W. H. Harman, C. J. Chang, *J. Am. Chem. Soc.* **2007**, *129*, 15128 – 15129; d) N. A. Piro, M. F. Lichterman, W. H. Harman, C. J. Chang, *J. Am. Chem. Soc.* **2011**, *133*, 2108 – 2111; e) G. T. Sazama, T. A. Betley, *Organometallics* **2011**, *30*, 4315 – 4319; f) G. E. Greco, R. R. Schrock, *Inorg. Chem.* **2001**, *40*, 3850 – 3860; g) E. M. Matson, Y. J. Park, A. R. Fout, *J. Am. Chem. Soc.* **2014**, *136*, 17398 – 17401; h) T. Taguchi, R. Gupta, B. Lassalle-Kaiser, D. W. Boyce, V. K. Yachandra, W. B. Tolman, J. Yano, M. P. Hendrich, A. S. Borovik, *J. Am. Chem. Soc.* **2012**, *134*, 1996 – 1999; i) B. M. Gardner, G. Balázs, M. Scheer, F. Tuna, E. J. L. McInnes, J. McMaster, W. Lewis, A. J. Blake, S. T. Liddle, *Angew. Chem. Int. Ed.* **2014**, *53*, 4484 – 4488; *Angew. Chem.* **2014**, *126*, 4573 – 4577; j) P. B. Duval, C. J. Burns, W. E. Buschmann, D. L. Clark, D. E. Morris, B. L. Scott, *Inorg. Chem.* **2001**, *40*, 5491 – 5496; k) A. J. Lewis, U. J. Williams, J. M. Kikkawa, P. J. Carroll, E. J. Schelter, *Inorg. Chem.* **2011**, *50*, 4660.

[8] U. J. Williams, J. R. Robinson, A. J. Lewis, P. J. Carroll, P. J. Walsh, E. J. Schelter, *Inorg. Chem.* **2014**, *53*, 27 – 29.

[9] J. A. Bogart, C. A. Lippincott, P. J. Carroll, E. J. Schelter, *Angew. Chem. Int. Ed.* **2015**, *54*, 8222 – 8225; *Angew. Chem.* **2015**, *127*, 8340 – 8343.

[10] J. A. Bogart, A. J. Lewis, S. A. Medling, N. A. Piro, P. J. Carroll, C. H. Booth, E. J. Schelter, *Inorg. Chem.* **2013**, *52*, 11600 – 11607.

[11] H. Zheng, S. J. Yoo, E. Münck, L. Que, *J. Am. Chem. Soc.* **2000**, *122*, 3789 – 3790.

[12] U. J. Williams, J. R. Robinson, A. J. Lewis, P. J. Carroll, P. J. Walsh, E. J. Schelter, *Inorg. Chem.* **2013**, *52*, 4142.

[13] P. Dröse, J. Gottfriedsen, C. G. Hrib, P. G. Jones, L. Hilfert, F. T. Edelmann, *Z. Anorg. Allg. Chem.* **2011**, *637*, 369 – 373.

[14] W. J. Evans, J. M. Perotti, R. J. Doedens, J. W. Ziller, *Chem. Commun.* **2001**, 2326 – 2327.

[15] R. Shannon, *Acta Crystallogr. Sect. A* **1976**, *32*, 751 – 767.

[16] The complexes would precipitate too quickly as microcrystalline needles.

[17] O. Eisenstein, P. B. Hitchcock, A. G. Hulkes, M. F. Lappert, L. Maron, *Chem. Commun.* **2001**, 1560 – 1561.

[18] a) C. H. Booth, M. D. Walter, M. Daniel, W. W. Lukens, R. A. Andersen, *Phys. Rev. Lett.* **2005**, *95*, 267202; b) W. W. Lukens, N. Magnani, C. H. Booth, *Inorg. Chem.* **2012**, *51*, 10105 – 10110.

[19] M. A. Boreen, J. A. Bogart, P. J. Carroll, E. J. Schelter, *Inorg. Chem.* **2015**, *54*, 9588 – 9593.

[20] N. G. Connelly, W. E. Geiger, *Chem. Rev.* **1996**, *96*, 877 – 910.

[21] M. W. Löble, J. M. Keith, A. B. Altman, S. C. E. Stieber, E. R. Batista, K. S. Boland, S. D. Conradson, D. L. Clark, J. Lezama Pacheco, S. A. Kozimor, R. L. Martin, S. G. Minasian, A. C. Olson, B. L. Scott, D. K. Shuh, T. Tyliszczak, M. P. Wilkerson, R. A. Zehnder, *J. Am. Chem. Soc.* **2015**, *137*, 2506 – 2523.

[22] I. Chávez, A. Alvarez-Carena, E. Molins*, A. Roig, W. Maniukiewicz, A. Arancibia, V. Arancibia, H. Brand, J. Manuel Manríquez, *J. Organomet. Chem.* **2000**, *601*, 126 – 132.

[23] R. R. Schrock, L. G. Sturgeoff, P. R. Sharp, *Inorg. Chem.* **1983**, *22*, 2801 – 2806.

[24] D. C. Bradley, J. S. Ghotra, F. A. Hart, *J. Chem. Soc. Dalton Trans.* **1973**, 1021 – 1023.

[25] R. K. Thomson, B. L. Scott, D. E. Morris, J. L. Kiplinger, *C. R. Chim.* **2010**, *13*, 790 – 802.

[26] Bruker (2009) SAINT. Bruker AXS Inc., Madison, Wisconsin, USA.

[27] Bruker (2009) SHELXTL. Bruker AXS Inc., Madison, Wisconsin, USA.

[28] Sheldrick, G. M. (2008) TWINABS. University of Gottingen, Germany.

[29] Sheldrick, G. M. (2007) SADABS. University of Gottingen, Germany.

[30] G. Sheldrick, *Acta Crystallogr. Sect. A* **2008**, *64*, 112 – 122.

[31] C. H. Booth, M. D. Walter, D. Kazhdan, Y.-J. Hu, W. W. Lukens, E. D. Bauer, L. Maron, O. Eisenstein, R. A. Andersen, *J. Am. Chem. Soc.* **2009**, *131*, 6480 – 6491.

[32] Gaussian 09, Revision D.01, Frisch, M. J.; Trucks, G. W.; Schlegel, H. B.; Scuseria, G. E.; Robb, M. A.; Cheeseman, J. R.; Scalmani, G.; Barone, V.; Mennucci, B.; Petersson, G. A.; Nakatsuji, H.; Caricato, M.; Li, X.; Hratchian, H. P.; Izmaylov, A. F.; Bloino, J.; Zheng, G.; Sonnenberg, J. L.; Hada, M.; Ehara, M.; Toyota, K.; Fukuda, R.; Hasegawa, J.; Ishida, M.; Nakajima, T.; Honda, Y.; Kitao, O.; Nakai, H.; Vreven, T.; Montgomery, Jr., J. A.; Peralta, J. E.; Ogliaro, F.; Bearpark, M.; Heyd, J. J.; Brothers, E.; Kudin, K. N.; Staroverov, V. N.; Kobayashi, R.; Normand, J.; Raghavachari, K.; Rendell, A.; Burant, J. C.; Iyengar, S. S.; Tomasi, J.; Cossi, M.; Rega, N.; Millam, N. J.; Klene, M.; Knox, J. E.; Cross, J. B.; Bakken, V.; Adamo, C.; Jaramillo, J.; Gomperts, R.; Stratmann, R. E.; Yazyev, O.; Austin, A. J.; Cammi, R.; Pomelli, C.; Ochterski, J. W.; Martin, R. L.; Morokuma, K.; Zakrzewski, V. G.; Voth, G. A.; Salvador, P.; Dannenberg, J. J.; Dapprich, S.; Daniels, A. D.; Farkas, Ö.; Foresman, J. B.; Ortiz, J. V.; Cioslowski, J.; Fox, D. J. Gaussian, Inc., Wallingford CT, **2009**.

[33] a) X. Cao, M. Dolg, *J. Mol. Struct.* **2002**, *581*, 139 – 147; b) M. Dolg, H. Stoll, H. Preuss, *J. Chem. Phys.* **1989**, *90*, 1730 – 1734.

[34] W. J. Hehre, R. Ditchfield, J. A. Pople, *J. Chem. Phys.* **1972**, *56*, 2257 – 2261.

[35] E. D. Glendening, J. K. Badenhoop, A. E. Reed, J. E. Carpenter, J. A. Bohmann, C. M. Morales, C. R. Landis, F. Weinhold, in *NBO 6.0*, Madison, WI., **2013**.

[36] a) S. I. Gorelsky, A. B. P. Lever, *J. Organomet. Chem.* **2001**, *635*, 187 – 196; b) S. I. Gorelsky, *AOMix: Program for Molecular Orbital Analysis*, http://www.sg-chem.net/, University of Ottawa, version 6.5, **2011**.

[37] Chemcraft. www.chemcraftprog.com.

Received: July 27, 2015
Published online on October 27, 2015